

## Isolation of Herpes Simplex Virus Procapsids from Cells Infected with a Protease-Deficient Mutant Virus

WILLIAM W. NEWCOMB,<sup>1</sup> BENES L. TRUS,<sup>2,3</sup> NAIQIAN CHENG,<sup>2</sup> ALASDAIR C. STEVEN,<sup>2</sup> AMY K. SHEAFFER,<sup>4</sup>  
DANIEL J. TENNEY,<sup>4</sup> SANDRA K. WELLER,<sup>5</sup> AND JAY C. BROWN<sup>1\*</sup>

*Department of Microbiology, University of Virginia Health Sciences Center, Charlottesville, Virginia 22908<sup>1</sup>; Laboratory of Structural Biology, National Institute of Arthritis and Musculoskeletal and Skin Diseases,<sup>2</sup> and Computational Bioscience and Engineering Laboratory, Center for Information Technology,<sup>3</sup> National Institutes of Health, Bethesda, Maryland 20892; Bristol-Myers Squibb Pharmaceutical Research Institute, Wallingford, Connecticut 06492<sup>4</sup>; and Department of Microbiology, University of Connecticut Health Center, Farmington, Connecticut 06030<sup>5</sup>*

Received 1 September 1999/Accepted 10 November 1999

**Herpes simplex virus type 1 (HSV-1) capsid proteins assemble in vitro into spherical procapsids that differ markedly in structure and stability from mature polyhedral capsids but can be converted to the mature form. Circumstantial evidence suggests that assembly in vivo follows a similar pathway of procapsid assembly and maturation, a pathway that resembles those of double-stranded DNA bacteriophages. We have confirmed the above pathway by isolating procapsids from HSV-1-infected cells and characterizing their morphology, thermal sensitivity, and protein composition. Experiments were carried out with an HSV-1 mutant (*m100*) deficient in the maturational protease for which it was expected that procapsids—normally, short-lived intermediates—would accumulate in infected cells. Particles isolated from *m100*-infected cells were found to share the defining properties of procapsids assembled in vitro. For example, by electron microscopy, they were found to be spherical rather than polyhedral in shape, and they disassembled at 0°C, unlike mature capsids, which are stable at this temperature. A three-dimensional reconstruction computed at 18-Å resolution from cryoelectron micrographs showed *m100* procapsids to be structurally indistinguishable from procapsids assembled in vitro. In both cases, their predominant components are the four essential capsid proteins: the major capsid protein (VP5), the scaffolding protein (pre-VP22a), and the triplex proteins (VP19C and VP23). VP26, a small, abundant but dispensable capsid protein, was not found associated with *m100* procapsids, suggesting that it binds to capsids only after they have matured into the polyhedral form. Procapsids were also isolated from cells infected at the nonpermissive temperature with the HSV-1 mutant *tsProt.A* (a mutant with a thermoreversible lesion in the protease), and their identity as procapsids was confirmed by cryoelectron microscopy. This analysis revealed density on the inner surface of the procapsid scaffolding core that may correspond to the location of the maturational protease. Upon incubation at the permissive temperature, *tsProt.A* procapsids transformed into polyhedral, mature capsids, providing further confirmation of their status as precursors.**

Herpes simplex virus type 1 (HSV-1) is widely distributed in the human population, where it is the etiological agent of recurrent fever blisters. Infection in neonates can result in more severe, disseminated disease (50). Like all herpesviruses, HSV-1 consists of an icosahedral capsid surrounded by a membrane envelope with the double-stranded DNA (dsDNA) genome contained inside the capsid. During HSV-1 infection, the capsid plays a central role in delivering the virus genome to the host cell nucleus. Following fusion of virus and host cell membranes, the DNA-filled capsid enters the peripheral cytoplasm. From there it is transported to the nucleus, where it docks at a nuclear pore and releases its DNA into the nucleoplasm (35, 38).

Progeny HSV-1 capsids are assembled in the nucleus, where they are also packaged with DNA before further virus maturation takes place (15, 33, 35). Capsids are initially formed with an internal protein scaffold (composed of UL26 and UL26.5 gene products) which is lost from the capsid upon DNA packaging. The scaffold contains the virus protease (UL26 gene), which cleaves both itself (to generate capsid proteins VP24 and

VP21) and the UL26.5 gene product (generating VP22a). The protease is essential for DNA packaging, capsid maturation, and virus growth (12).

The events of capsid formation prior to DNA encapsidation have been examined in insect cell extracts containing capsid proteins and in a purified system in which capsids are formed from purified proteins (24–26, 42). Studies with such systems show that mature, icosahedral capsids can be assembled from the major capsid protein (VP5), the two triplex proteins (VP19C and VP23), and a scaffolding protein (e.g., pre-VP22a). Further, the mature capsid is found to be assembled by way of a spherical, more fragile intermediate called the procapsid. Apart from a minor difference in the scaffolding protein (pre-VP22a is not cleaved in the procapsid [24]), the procapsid has the same protein composition as the mature capsid formed in vitro. The procapsid differs, however, in important respects: (i) the procapsid is spherical in overall morphology whereas the mature capsid is icosahedral; (ii) the procapsid is a more porous structure, having holes between capsomers that are sealed in the mature capsid; (iii) many procapsid hexons are oval in cross section whereas those of the mature capsid are hexagonal (46); and (iv) procapsids are disassembled after incubation at 4°C whereas mature capsids are unaffected. Procapsids transform into mature capsids in a process in which the shell undergoes the structural changes

\* Corresponding author. Mailing address: Department of Microbiology, Box 441, University of Virginia Health Sciences Center, Charlottesville, VA 22908. Phone: (804) 924-1814. Fax: (804) 982-1071. E-mail: JCB2G@VIRGINIA.EDU.

outlined above, and the scaffold disengages from the surface shell and is either expelled or retracted into a smaller core structure. In vivo, this transformation is dependent on the presence and activity of the maturational protease (5, 12, 30, 34).

Formation of capsids in vitro by way of the procapsid intermediate suggests that the same intermediate may be found in vivo, and Rixon and McNab have recently provided evidence this is the case (34). Electron micrographs of cells infected with HSV-1 *ts1201* showed that the capsids accumulating at the nonpermissive temperature (NPT) were spherical like procapsids and sensitive to disassembly when the cells were incubated at 0°C. To clarify the properties of procapsids present in infected cells, we isolated them by antibody precipitation from infected cell lysates and examined them by electron microscopy, sensitivity to disruption at 0°C, and sodium dodecyl sulfate (SDS)-polyacrylamide gel electrophoresis. Experiments were carried out with an HSV-1 mutant (*m100*) in which procapsids are expected to accumulate due to the absence of the maturational protease (12). The results as described below show that procapsids isolated from infected cells are essentially the same particles as procapsids assembled in vitro.

#### MATERIALS AND METHODS

**Cells and viruses.** *m100* and *tsProt.A* viruses were isolated by Min Gao and his colleagues, who generously provided both viruses for this study (12). Previously described procedures were used for growing *m100* on the complementing cell line, BMS-MG22 (12). Stock virus titers were in the range of  $5 \times 10^8$  to  $1 \times 10^9$  PFU/ml. Wild-type HSV-1 (strain 17MP) and *tsProt.A* were propagated on monolayer cultures of BHK or Vero cells that were grown in minimal essential medium containing 10% fetal calf serum and antibiotics. HSV-1 A and B capsids were isolated as previously described (27) from infected BHK cells.

**Procapsid isolation.** *m100* procapsids were isolated from BHK cells that were infected in 150-cm<sup>2</sup> plastic flasks at a multiplicity of infection of 10 and incubated for 15 h at 37°C, during which time cells became detached from the substrate. All subsequent steps were carried out at room temperature (~21°C). Cells from one to two flasks (~ $2 \times 10^8$  cells) were harvested by low-speed centrifugation, suspended in 1 ml of phosphate-buffered saline (PBS), and lysed by sonication in a probe sonicator (Ultrasonics, Inc., model W-375; setting 3; two cycles of ~8 s each). Protease inhibitors (aprotinin, leupeptin, and Pefabloc; 1/10 volume of a stock solution prepared by dissolving 1 tablet of Boehringer Mannheim Complete, Mini in 1 ml of PBS) were then added, and sedimentable material was removed by centrifugation for 6 min at  $16,000 \times g$ . Procapsids were then precipitated from the lysate by addition of 50  $\mu$ l of VP5-specific monoclonal antibody (Mab) 6F10 (4 mg/ml) (24, 39) followed by incubation for 5 min at room temperature. Precipitates were harvested by centrifugation for 2 min at  $16,000 \times g$ , resuspended in 200  $\mu$ l of PBS, and subjected to two further cycles of antibody precipitation as described above. Most preparations yielded 100 to 200  $\mu$ l of procapsids at a concentration of ~1 mg/ml, and these were used for structural and biochemical analyses as described below.

**Cryo-electron microscopy and image reconstruction.** Immunoprecipitated procapsids were prepared for cryo-electron microscopy by adsorption onto a thin carbon film (supported on a thick holey carbon film) and freezing as previously described (25, 54). The same procedures were used for A capsids except that specimens were not immunoprecipitated. Micrographs were recorded on a Philips CM200-FEG electron microscope at a magnification of  $\times 38,000$ , using minimal electron dose methods producing radiation levels of ~8 electrons/ $\text{\AA}^2$ .

Three-dimensional reconstructions of procapsids and A capsids were computed beginning with micrographs that were selected for analysis by visual appraisal (e.g., to assess density of particles and contrast) and by optical diffraction to assess the state of defocus and resolution. For *m100* procapsids, two micrographs whose first contrast transfer function (CTF) zeros were  $1/29.7 \text{\AA}^{-1}$  and  $1/24.7 \text{\AA}^{-1}$  were scanned at 17  $\mu\text{m}/\text{pixel}$  on a Perkin-Elmer 1010MG microdensitometer, yielding an effective pixel size of ~4.6  $\text{\AA}$ . CTF correction consisted of simple phase flipping (48). A total of 410 images were processed as previously described (46). For *tsProt.A* procapsids, 160 images from 13 micrographs (with CTF zeros between  $1/22$  and  $1/26 \text{\AA}^{-1}$ ) were analyzed to a resolution of 28  $\text{\AA}$  after scanning at 25  $\mu\text{m}/\text{pixel}$ , yielding an effective pixel size of ~6.9  $\text{\AA}$ . For A capsids, 1,488 images from 14 micrographs (with CTFs zeros between  $1/18$  and  $1/25 \text{\AA}^{-1}$ ) were analyzed to 18- $\text{\AA}$  resolution. Three-dimensional structures were solved by the polar Fourier transform method (1), with our earlier reconstructions (46) as starting models. After iterative cycles of refinement of orientation angles and origins, images with the highest correlation coefficients were selected and a density map was calculated (11). Calculations were performed with 338, 89, and 907 images for *m100* procapsids, *tsProt.A* procapsids, and A capsids, respectively. The resolution of the resulting reconstructions was 18  $\text{\AA}$  for *m100* pro-

capsids and A capsids and 28  $\text{\AA}$  for *tsProt.A* procapsids as assessed by the FRC3D criterion (6).

**SDS-polyacrylamide gel electrophoresis and Western immunoblotting.** Previously described procedures were used for SDS-polyacrylamide gel electrophoresis followed by Coomassie blue staining (23). Stained bands were determined quantitatively by scanning the gel in a flatbed scanner followed by densitometric analysis using ImageQuant software. Specimens to be examined by SDS-polyacrylamide gel electrophoresis and Western immunoblotting were precipitated with 10% trichloroacetic acid, resuspended in loading buffer (200 mM Tris-HCl, 100 mM dithiothreitol, 2% SDS, 10% glycerol [pH 8.8]), boiled for 3 min, and separated by electrophoresis on 4 to 20% polyacrylamide gradient gels. Proteins were electrophoretically transferred to nitrocellulose membranes, washed twice in Tris-buffered saline (20 mM Tris-HCl, 500 mM NaCl [pH 7.5]), blocked for 60 min in blocking buffer (Tris-buffered saline plus 0.2% nonfat dry milk), and processed by using an Immunostar chemiluminescence detection kit (Bio-Rad) as directed by the manufacturer. Primary antibodies were diluted in blocking buffer plus 0.1% Tween 20 and added to blots for 2 h at the following dilutions: VP5, Mab 13-183 (Advanced Biotechnologies Inc.), 1:1,000; VP23, Mab 1D2 (see below), 1:2,000; UL26.5 gene products, Mab MCA406 (Serotec, Inc.), 1:10,000; VP19C, rabbit polyclonal antibody NC2 (49), 1:10,000; VP26, rabbit polyclonal antibody R31/B3 (22), 1:500; and actin, mouse monoclonal clone C4 (ICN Pharmaceuticals), 1:500. Blots were then treated for 2 h with alkaline phosphatase-conjugated secondary antibodies, either goat anti-mouse or goat anti-rabbit immunoglobulin G (BioRad) (1:4,000 dilution) and developed with an Immunostar chemiluminescence detection kit. Labeled bands were detected by exposing blots to Kodak XAR-5 film.

**VP23-specific Mab 1D2.** A mouse hybridoma cell line secreting Mab 1D2 was isolated by the procedures described previously for immunization of BALB/c mice and for fusion of spleen cells with Sp2/O-Ag14 myeloma cells (24). The immunogen was VP23 that had been purified biochemically from lysates of Sf9 cells expressing VP23 as a result of infection with a recombinant baculovirus (BAC-UL18) encoding VP23 (45). Beginning with the cell lysate, purification was accomplished by ammonium sulfate precipitation followed by cation-exchange chromatography as described previously for purification of triplexes (25). Hybridoma cell lines were screened by enzyme-linked immunosorbent assay (9) using VP23-containing Sf9 cell extracts as antigen. The antibody secreted by hybridoma cell line 1D2 was found to be specific for VP23 by enzyme-linked immunosorbent assay and by Western immunoblot assays. Previously described procedures were used for growing the 1D2 hybridoma cells as an ascites and for purifying the antibody (immunoglobulin G1 subclass) from the ascites fluid (10). Experiments were performed beginning with a stock solution of antibody whose concentration was 2.8 mg/ml.

**Electron microscopy.** Procapsid-containing precipitates were prepared for electron microscopy by fixation, embedding in Epon 812, and thin sectioning as described previously (20, 24). Negative staining with 1% uranyl acetate was carried out as described by Thomas et al. (44). All electron micrographs of thin-sectioned or negatively stained specimens were recorded on a JEOL 100CS transmission electron microscope operated at 80 keV.

#### RESULTS

Efforts to isolate procapsids from HSV-1-infected cells are expected to be influenced by the fact that the procapsid is an assembly intermediate present only transiently during formation of the more stable, mature capsid (24). Procapsids are therefore expected in lower abundance than mature capsids. To address this problem, our studies were carried out with a protease-deficient HSV-1 mutant because cells infected with protease-defective viruses are found to accumulate large-cored B capsids (12, 30), structures that we interpret to be procapsids. Also, experience with capsid assembly in cell extracts has indicated that while the protease is not required for production of mature, icosahedral capsids, its presence significantly enhances conversion of the procapsid to the mature form (26).

*m100* was considered an appropriate protease-deficient mutant for this study because while the protease domain of its parent gene is lacking, the scaffolding protein region (i.e., the UL26.5 gene) is present and functions normally (12). To isolate procapsids, cells were infected with *m100* virus and lysed by sonication, and the lysates were treated with VP5-specific Mab 6F10, a treatment that precipitates procapsids (24). Precipitated procapsids were then examined by electron microscopy, SDS-polyacrylamide gel electrophoresis and tests to evaluate their sensitivity to disassembly at 0°C.

**Electron microscopy.** Figure 1b shows a thin-section electron micrograph of a procapsid-containing precipitate. In such preparations, *m100* procapsids were found to be round or slightly irregular in overall shape, with distinct shell and core layers. The images of precipitated procapsids (Fig. 1b) were similar to those of procapsids seen in infected cell nuclei (Fig. 1a) (12, 30), suggesting that the isolation process did not markedly alter procapsid morphology.

In negatively stained preparations (Fig. 1c), nearly all *m100* procapsids were seen to be uniform in structure and round in profile, suggesting that they are spherical in shape. The round profile contrasts with that of HSV-1 B capsids (Fig. 1d), where distinct angles, indicative of a polyhedral morphology, are evident. Capsomers could be seen in most images of negatively stained procapsids (Fig. 1c). Micrographs of both thin-sectioned and negatively stained specimens indicated that most procapsids were intact. It was rare to see fragments of procapsids such as might arise from incomplete procapsid assembly or from fragmentation of complete procapsids (Fig. 1a to c).

Images of procapsids preserved in the frozen hydrated state also indicated that they have a uniform, spherical morphology with distinct shell and core layers (Fig. 1e). The measured procapsid diameter in such images was  $124 \pm 3$  nm ( $n = 46$ ), and capsomers could be seen in most individual procapsids (e.g., second procapsid from the right in Fig. 1e).

**Three-dimensional reconstruction.** Images of cryopreserved specimens such as those shown in Fig. 1e were used to compute a three-dimensional reconstruction of the *m100* procapsid. A total of 338 procapsid images were included in the reconstruction which was computed by the polar Fourier transform method as previously described (1, 46) to a resolution of 18 Å. A surface-shaded view of the reconstruction is shown in Fig. 2a viewed along an axis of twofold symmetry. The vertical line down the center of the image divides it into halves in which irregular density associated with antibodies bound to the tips of the capsomers has been computationally removed in the right half of the image. The irregularity of this density may be assigned to both partial occupancy and flexibility of the antibodies about their points of attachment to the capsid.

To examine the *m100* procapsid reconstruction, we find it helpful to start with the hexon at the center of the image (i.e., the hexon on the icosahedral twofold axis). Moving laterally to the right, one encounters a P hexon with the oval morphology characteristic of procapsid hexons (Fig. 3) (46). Further to the right is a penton, identifiable because it has five rather than six subunits. Proceeding upward and to the left, one sees a row of three hexons followed by a penton near 12 o'clock. A face hexon (C hexon [40]) can be identified in the angle created by the excursion described above.

For comparison with the *m100* procapsid, Fig. 2 shows a reconstruction of the HSV-1 A capsid (Fig. 2d) and the reconstruction described earlier of the procapsids assembled in vitro from extracts of insect cells containing HSV-1 proteins (Fig. 2c) (24). All reconstructions are viewed along the icosahedral twofold axis. Comparison of the three structures shows that whereas the A capsid is icosahedral in overall shape, the two procapsids are spherical with no evidence of angularity. Examination of capsomer morphology also emphasizes the similarity of *m100* and in vitro procapsids. For example, the P hexon is found to be oval in the two procapsid reconstructions (Fig. 2a and c), whereas it is hexagonal in the A capsid (Fig. 2d). The same comparison is shown at higher magnification in Fig. 4a (*m100* procapsid) and b (A capsid).

Comparison of the reconstructions shows that the porous nature of procapsids assembled in vitro is also seen in *m100* procapsids. For example, whereas a set of six small holes (black

spots) surrounds the twofold axis hexon (E hexon) in both procapsid reconstructions, all are sealed in the A capsid (compare Fig. 2a and c with 2d and Fig. 4a with 4b). Similarly, holes surrounding the pentons in both procapsids are not seen in A-capsid pentons (compare Fig. 4c and d).

***tsProt.A* procapsids.** Procapsids were also isolated from cells infected with HSV-1 mutant *tsProt.A*. This mutant, constructed to contain the same amino acid changes found in *ts1201* (12, 30), lacks function of the UL26-encoded protease when grown at the NPT (39°C), and so procapsids are expected to accumulate (5, 12, 30, 34). To isolate *tsProt.A* procapsids, therefore, cells were infected with *tsProt.A* at the NPT, and procapsids were harvested by antibody precipitation as described above for cells infected with *m100*. Electron microscopy of such procapsids supports the view that their structure is that of the procapsid and distinct from the mature capsid. For example, in both negatively stained and frozen hydrated preparations, *tsProt.A* procapsids appear round rather than angular in profile, suggesting the spherical procapsid morphology (data not shown).

A three-dimensional reconstruction computed from cryomicrographs of *tsProt.A* procapsids showed that they have the same basic structural features as in vitro and *m100* procapsids. These include a spherical morphology, porous shell, and asymmetric hexons—oval in the case of P and E hexons and triangular in the case of C hexons (compare Fig. 2b with 2a and c). Like *m100* procapsids, *tsProt.A* procapsids were found to be distinct in these features from mature capsids which are polyhedral and closed and have symmetric hexons (compare Fig. 2b with 2d). Although close comparison of the *tsProt.A* and *m100* procapsids suggests subtle differences, at the present state of analysis these may be attributed to the lower resolution of the *tsProt.A* reconstruction (28 Å vs. 18 Å, and 89 particles vs. 338 particles) and perhaps to a slight difference in incipient maturation (see Discussion).

Spherical internal scaffolds are present in both *m100* and *tsProt.A* procapsids, as in procapsids assembled in vitro (25, 46). In cryomicrographs (e.g., Fig. 1e), this feature appears as an inner ring of projected density. In the reconstructed density maps, there is very little contrast to differentiate local features within the capsid shell (data not shown), and such a density distribution could, in principle, arise from icosahedral averaging of a nonsymmetric structure. Thus, the question of whether the scaffold is icosahedrally symmetric remains unsettled. Nevertheless, the radial distribution of density through the procapsid, including the scaffold, may be examined by calculating spherically averaged radial density profiles from the corresponding three-dimensional density maps, and these are shown in Fig. 5.

The profiles can be considered to consist of three regions: (i) a region from a radial distance of ~480 to 640 Å corresponding to the procapsid shell, (ii) a scaffold region from ~180 to 480 Å, and (iii) an inner region inside a radius of 180 Å. The density profiles were found to be quite similar for the three procapsid reconstructions, particularly in the shell layer, which was found to have almost exactly the same thickness and radial distance from the center in the three reconstructions. The radius of the external procapsid edge, for example, differed by less than 20 Å among the three procapsids. Three peaks of density were found in the shell region of each procapsid type. The scaffold region was also similar among the three reconstructions, showing three major peaks of density. Among the three procapsid types, the major difference was prominent density in the inner region of *tsProt.A* procapsids (radial distance of ~100 to 160 Å) that was absent in the profiles of in vitro and *m100* procapsids.

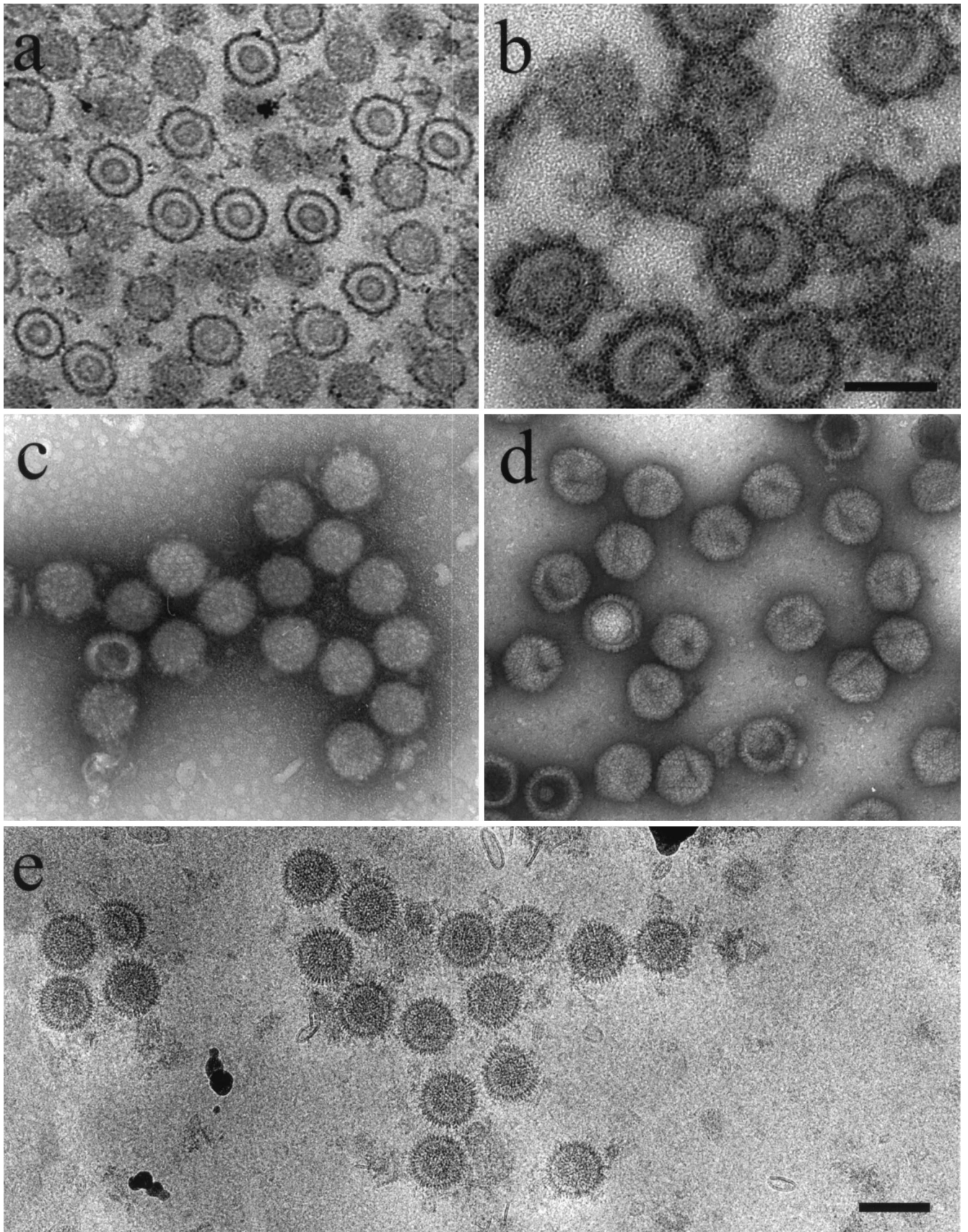


FIG. 1. Electron microscopy of HSV-1 procapsids. (a) Thin section showing procapsids in the nucleus of a BHK cell infected for 15 h with HSV-1 mutant *m100*; (b) thin section preparation of *m100* procapsids after isolation by antibody precipitation; (c) *m100* procapsids after negative staining with uranyl acetate; (d) negatively stained HSV-1 B-capsids; (e) *m100* procapsids preserved in the frozen hydrated state. Note that *m100* procapsids are round in profile (c and e) and consist of distinct shell and core layers. All micrographs are shown at the same magnification (bar = 1,500 Å) except for panel b (bar = 1,000 Å).

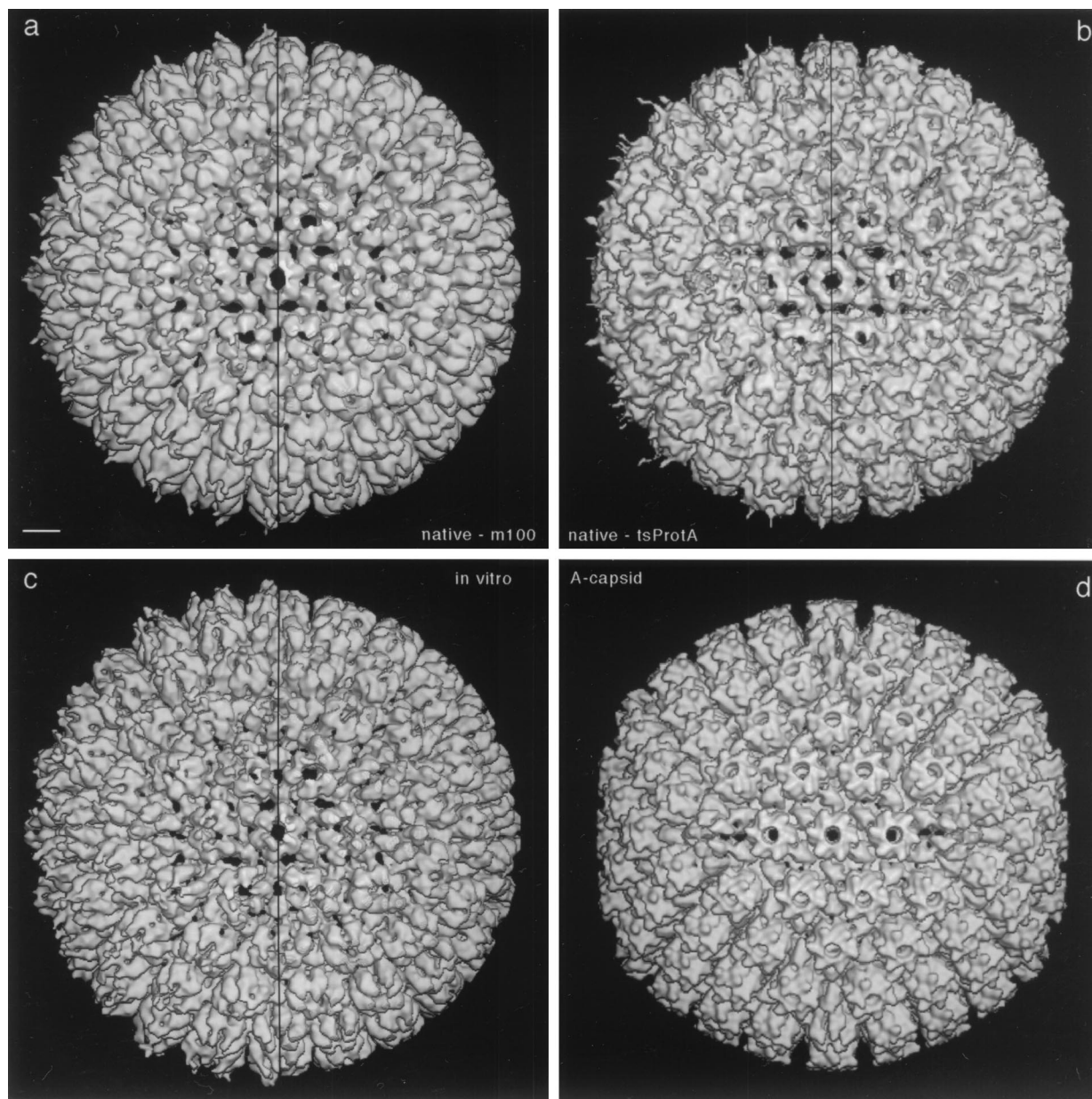


FIG. 2. Three-dimensional reconstructions of HSV-1 procapsids from three different sources (a to c) compared to the mature capsid (d). (a) Native procapsids isolated from BHK cells infected with the mutant *m100*; (b) native procapsids isolated from BHK cells infected at the NPT temperature with *tsProt.A*; (c) procapsids assembled *in vitro* from lysates of Sf9 cells containing HSV-1 capsid proteins (reproduced from reference 46); (d) native A capsids isolated from BHK cells infected with wild-type HSV-1. All reconstructions are shown in surface-shaded representations as viewed along the icosahedral twofold axis of symmetry. To facilitate comparison, the reconstructions shown in panels a and d were restricted to 25-Å resolution, which is similar to the values for the reconstructions in panels b (~28-Å resolution) and c (~27-Å resolution). To isolate and concentrate the fragile procapsids for cryoelectron microscopy, they were precipitated with MAb 6F10 as described in Materials and Methods (24, 39). In consequence, some antibody-associated density is present around their peripheries in these density maps. The maps are represented both with this density present (left half of each panel) and with it computationally removed (right half) by setting the density to background outside a radius of ~640 Å. Note that the three procapsids are essentially identical in structure. Bar = 100 Å.

**Procapsid maturation.** Both *m100* and *tsProt.A* procapsids were tested for the ability to transform *in vitro* into the mature, icosahedral capsid morphology. Tests were carried out with procapsids that were suspended in PBS at a concentration of approximately 0.5 mg/ml, incubated at room temperature (21°C), and tested by electron microscopy for their conversion to the mature capsid morphology. High proportions (greater than 80%) of both *m100* and *tsProt.A* procapsids were found to be transformed in most experiments. Figure 6, for example, shows the results obtained with *tsProt.A* procapsids before

(Fig. 6a) and after (Fig. 6b) incubation for 72 h at 21°C. Note that capsids were round in profile before incubation but angular afterward. Prolonged incubation at 21°C was required for procapsids to be transformed. It was rare to see any evidence of procapsid transformation prior to approximately 48 h of incubation, but most procapsids were converted by 60 to 72 h.

**Cold sensitivity.** The sensitivity of *m100* and *tsProt.A* procapsids to dissociation following incubation at 0°C was tested by electron microscopy of negatively stained specimens. Procapsids found to be intact after incubation at room tempera-

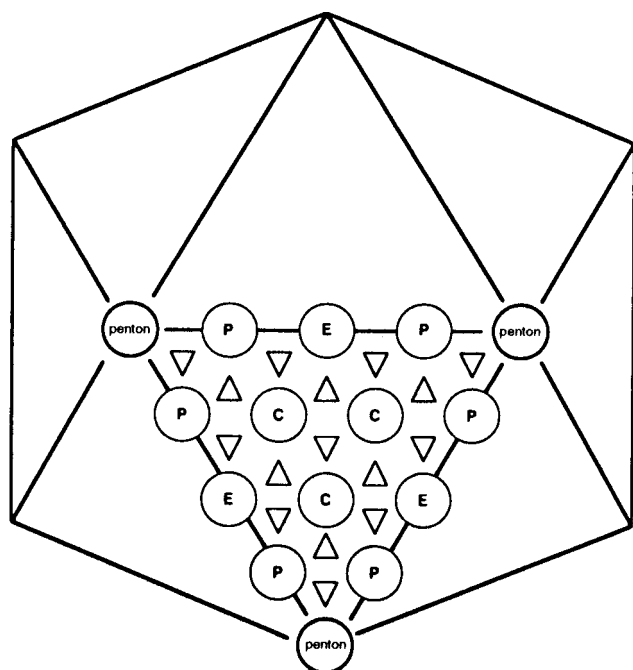


FIG. 3. Diagram showing the salient features of the  $T = 16$  surface lattice of herpesvirus capsids. Pentons (capsomers with five nearest neighbors) are at each of the 12 vertices. There are three classes of hexons (capsomers with six nearest neighbors) distinguished according to their lattice sites. A peripentonal hexon (P hexon) is adjacent to a penton; E hexons are at the middle of each edge and sit on icosahedral twofold axes; and three C hexons are found at the center of each facet (adapted from reference 40). At each trigonal site (a site of local or global threefold symmetry, surrounded by three capsomers) is a triplex (15, 41). These heterotrimeric complexes are indicated by small triangles. Triplexes may be subclassified according to their positions on the surface lattice (52).

ture ( $21^{\circ}\text{C}$ ) or  $0^{\circ}\text{C}$  were counted as a measure of structural integrity. The results showed a marked decrease in the number of both *m100* and *tsProt.A* procapsids present after incubation at  $0^{\circ}\text{C}$ , suggesting they were dissociated at the cold temperature. Representative results for *m100* procapsids are shown in Table 1. No comparable decrease in the number of B capsids was observed after similar incubation at  $0^{\circ}\text{C}$ . Material found in micrographs of dissociated procapsids could not be interpreted to suggest any clear structural relationship to the parent procapsid (data not shown).

**Protein composition.** The protein composition of procapsids was determined by SDS-polyacrylamide gel electrophoresis followed by staining with Coomassie blue. The results shown in Fig. 7a demonstrated that both *m100* and *tsProt.A* procapsids contain the major capsid protein (VP5), the two triplex proteins (VP19C and VP23), and the scaffolding protein, pre-VP22a. Only the uncleaved form of the scaffolding protein (i.e., pre-VP22a) was detected in *m100* procapsids. In *tsProt.A* procapsids most of the scaffolding protein was uncleaved, but a trace of the cleaved form, VP22a, was observed. In addition to the proteins mentioned above, *tsProt.A* procapsids contained a small amount of a protein migrating with an apparent molecular mass of  $\sim 66$  kDa (labeled "protease" in Fig. 7a) and staining with a MAb (MCA406) specific for the UL26 and UL26.5 gene products (data not shown). We infer that this protein corresponds to the full-length UL26 gene product. No VP24 was found associated with *tsProt.A* procapsids. As expected, no 66-kDa protein was detected in *m100* procapsids. Neither *m100* nor *tsProt.A* procapsids were found to contain VP26 (Fig. 7a), a 12-kDa polypeptide found at the hexon tips in mature capsids (3, 53).

In addition to the capsid proteins described above, stained gels of both *m100* and *tsProt.A* procapsid proteins were found to contain a previously unrecognized protein migrating slightly more rapidly than pre-VP22a (starred band in Fig. 7a). In Western immunoblots, this protein stained positively with a MAb (clone C4; ICN Pharmaceuticals) specific for actin (data not shown). We assume therefore that the protein corresponds to actin and that it is derived from the BHK cells from which procapsids were isolated.

Antibodies specific for HSV-1 capsid proteins were used in Western immunoblotting to confirm the identities of the *m100* procapsid proteins described above. Bands identified as VP5, VP19C, pre-VP22a, and VP23 were found to react with specific antibodies as shown in Fig. 7b. No VP26 was detected by immunoblot analysis of *m100* procapsids, however, despite the fact that it was detected in control HSV-1 B capsids (Fig. 7) and in *m100*-infected cell extracts (data not shown).

Stained gels such as that shown in Fig. 7a were used to make quantitative measurements of the *m100* procapsid protein composition. Protein amounts were determined by densitometric scanning of stained gels, and copy numbers were estimated on the assumption that procapsids contain 960 copies of VP5, the number present in mature capsids (15, 27). Analysis was affected by the fact that during electrophoresis, VP19C migrates coincidentally with the heavy chain of the antibody used to precipitate procapsids. No quantitative measurement could therefore be made for VP19C. Pre-VP22a and actin bands were closely spaced, but resolution was sufficient to permit them to be determined separately. Protein copy numbers determined for pre-VP22a and VP23 were  $1,918 \pm 170$  ( $n = 4$ ) and  $730 \pm 308$  ( $n = 4$ ), respectively. For comparison, the VP23 copy number in mature capsids is 640 (15, 33, 41). Although no quantitative determination of VP19C could be obtained from Coomassie blue-stained gels, comparison of the intensities of the Western immunoblot signals confirmed that VP19C, and the other capsid shell proteins, were present at comparable levels in all capsid types (Fig. 7b).

The scaffolding protein content of *m100* procapsids was also determined beginning with the three-dimensional reconstruction shown in Fig. 2a. The mass in the scaffold region of the radial density profile was calculated by an appropriately weighted integral of the density above background in the scaffold region (between radii of 180 and 480 Å) and calibrated against the corresponding integral for the surface shell, which was taken to be 180.9 MDa (Table 2). Taking into account the molecular weight of pre-VP22a, the calculations yielded a copy number of 1,866 to 2,070 scaffolding protein molecules per procapsid depending on where the baseline of the radial density profile was set. Similar values were obtained earlier by radial integration of the reconstructions computed for procapsids assembled *in vitro* (Table 2). The range of values obtained for *m100* procapsids is in satisfactory agreement with the value,  $1,918 \pm 170$  pre-VP22a molecules/*m100* procapsid (see above), determined from gel electrophoresis of procapsid proteins.

## DISCUSSION

MAb 6F10 was used initially to isolate procapsids from lysates of *m100*-infected cells because it was found to be effective in precipitating procapsids formed *in vitro*. 6F10 also precipitates capsids with the mature morphology such as A and B capsids, but it appears to be particularly efficient in precipitating procapsids. Attempts were made to isolate *m100* and *tsProt.A* procapsids by sucrose density gradient centrifugation, but these efforts met with only limited success. Since antibody precipitation showed procapsids were present in infected cell

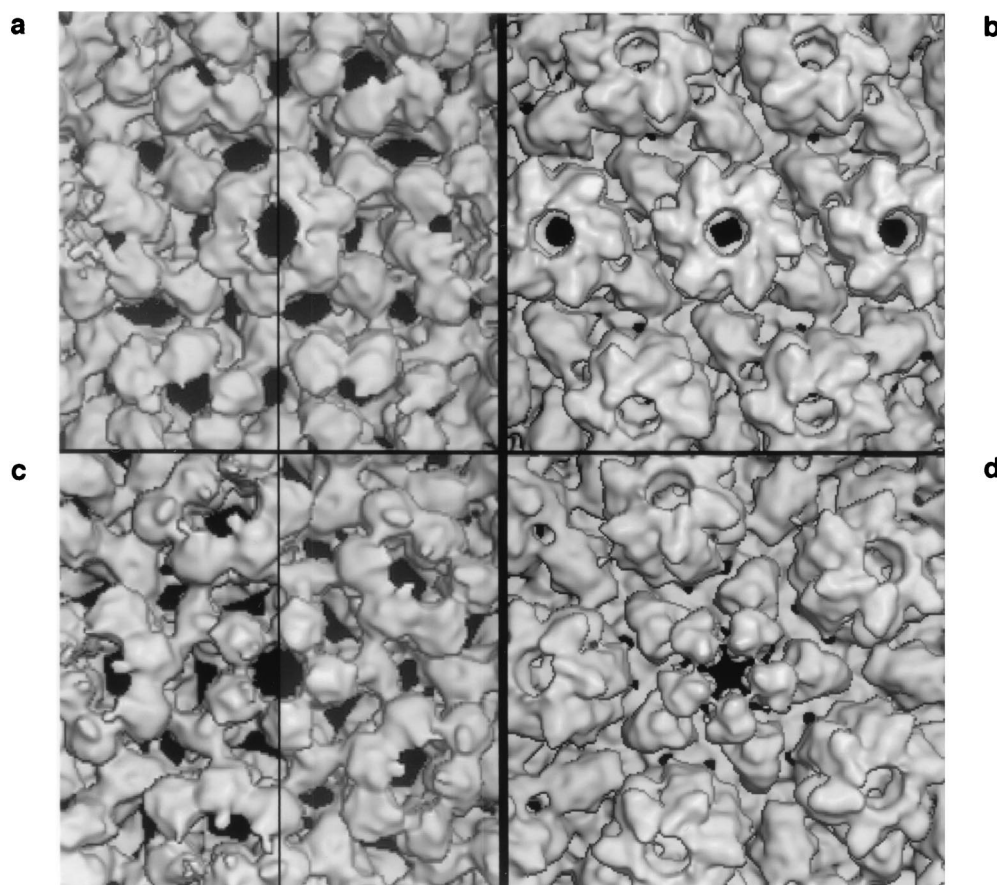


FIG. 4. The structural changes that accompany HSV-1 capsid maturation are characterized by comparing the hexons (a and b) and pentons (c and d) of the *m100* procapsid (a and c) and the mature capsid (A capsid; b and d). The outer surfaces are shown in each case. Panels a and b are centered on the E hexon which resides at each twofold axis and includes portions of the surrounding P and C hexons (for nomenclature, see the legend to Fig. 3). In the left halves of panels a and c, the less ordered density associated with the immunoprecipitating 6F10 antibodies is present, whereas it has been computationally removed in the right halves. The resolution is 18 Å. Bar = 100 Å.

lysates, we assume the procedures used for sucrose gradient isolation resulted in procapsid maturation, degradation, aggregation or disassembly.

**Procapsids assembled in vivo and in vitro are structurally indistinguishable.** Electron micrographs of *m100* (Fig. 1) and *tsProt.A* (data not shown) procapsids show structures with round profiles suggesting that they have the spherical morphology described earlier for procapsids assembled in vitro (24). It was rare to see capsids with angles in precipitates from *m100* or *tsProt.A*-infected cells. The very high proportion of procapsids compared to polyhedral capsids present in lysates of *m100*- and *tsProt.A*-infected cells supports the view that procapsids are the predominant capsid type that accumulates in infected cells lacking activity of the maturational protease (5, 7, 12, 24, 30, 34).

The three-dimensional reconstructions of *m100* and *tsProt.A* procapsids (Fig. 2a and b) revealed a wealth of structural information not present in images of negatively stained or thin-sectioned specimens. Of particular interest is the marked similarity of the *m100* procapsid structure with that of procapsids assembled in vitro from cell extracts (Fig. 2c). In the shell layer particularly, the *m100* and in vitro procapsid structures were found to be identical in even the subtlest features seen at the resolution of the current reconstructions (compare Fig. 2a and c). Such features include the structures of the hexons, the pentons, the triplexes, and holes through the capsid shell.

There can be little doubt therefore that the *m100* procapsid is the structural homolog of procapsids assembled in vitro. The homology is further emphasized by the cold sensitivity of *m100* procapsids (Table 1), a defining property of procapsids assembled in vitro (24, 25).

The three-dimensional reconstruction of *tsProt.A* procapsids shows they have the same basic structure as *m100* and in vitro procapsids. Such small differences as are seen between the respective density maps (e.g., a slightly more symmetrical hexon morphology in *tsProt.A* procapsids) may reflect either differing resolution or very early steps of maturation in *tsProt.A* procapsids. Such early maturation steps could be promoted by expression of a low level of protease function during procapsid isolation. The structure of the *tsProt.A* procapsid is of particular significance because it is known that *tsProt.A* procapsids can mature into infectious virions in vivo (5, 30, 34). Thus, maturability in vivo is a property of procapsids with the structure defined here for *m100* and *tsProt.A* procapsids.

**Procapsid protein composition.** The predominant protein components of *m100* and *tsProt.A* procapsids were found to be the same as those of procapsids assembled in vitro, namely, VP5, VP19C, VP23, and pre-VP22a. Apart from the presence of the protease in *tsProt.A* procapsids (Fig. 7a), in vivo procapsids did not contain any major protein species observable by Coomassie blue staining that was not also present in in vitro procapsids. The above observation was unexpected since in

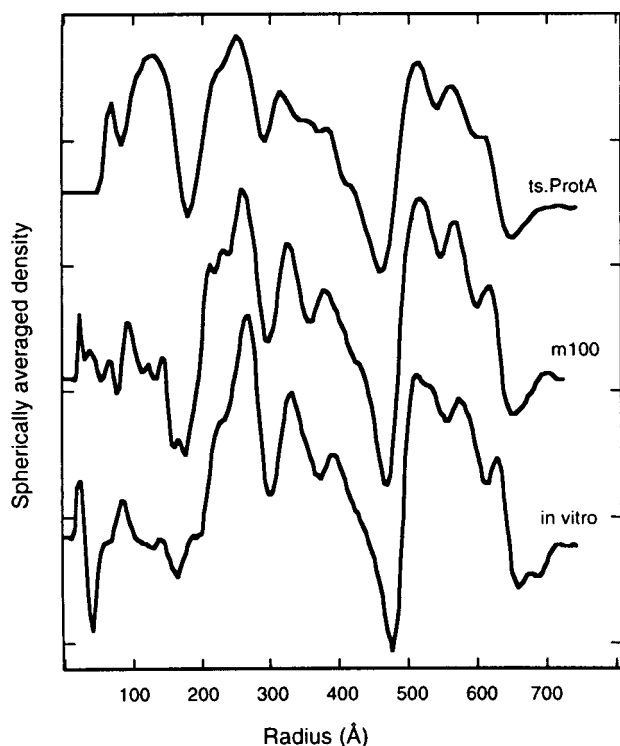


FIG. 5. Radial density profiles of HSV-1 procapsids from three sources: native procapsids isolated from BHK cells infected at the NPT with *tsProt.A* (top curve), native procapsids isolated from BHK cells infected with *m100* (middle), and procapsids assembled in vitro from lysates of Sf9 cells containing HSV-1 capsid proteins (bottom) (46). The profiles were calculated by spherical averaging of the corresponding three-dimensional density maps. The main features of the surface shell (three peaks between radii of 480 and 650 Å) and the scaffold (three peaks between radii of 200 and 460 Å) are well conserved. However, the *tsProt.A* procapsids are the only ones to show a significant density peak inside the scaffold shell suggested to correspond to the HSV-1 UL26 gene product, the virus protease.

vivo procapsids have the potential to mature into virions and might therefore contain proteins involved in DNA processing and packaging not found in procapsids formed in vitro. Since small amounts of DNA processing and packaging proteins, detectable in Western immunoblots, are found associated with intracellular mature capsids (e.g., B capsids [21, 36, 43, 51]), we have initiated immunoblot studies to attempt to detect them in procapsids derived from *m100*- and *tsProt.A*-infected cells.

VP26 is a small (12-kDa) protein located at the distal tips of HSV-1 capsid hexons (3, 46, 53). One VP26 molecule is bound to each VP5 in all 150 hexons, and so there are a total of 900 VP26 molecules in a mature capsid. Studies with an HSV-1 mutant lacking the gene (UL35) encoding VP26 have demonstrated that VP26 potentiates HSV-1 growth in neural cells in vivo but is not required for virus replication in cell culture (8). The protein analyses reported here consistently failed to detect VP26 in either *m100* or *tsProt.A* procapsids despite the fact that the same methods revealed its presence in B capsids (Fig. 7) and in the cells from which *m100* and *tsProt.A* procapsids were isolated (data not shown). We conclude that VP26 is not a component of the HSV-1 procapsid. Since it is present in virions and in mature capsids, it must be added after procapsids are formed. The function of VP26 in capsids must be expressed in a process (e.g., DNA packaging or addition of tegument) that occurs as the mature capsid is formed or thereafter.

SDS-polyacrylamide gel analysis of *m100* and *tsProt.A* procapsid precipitates demonstrated the presence of a band cor-

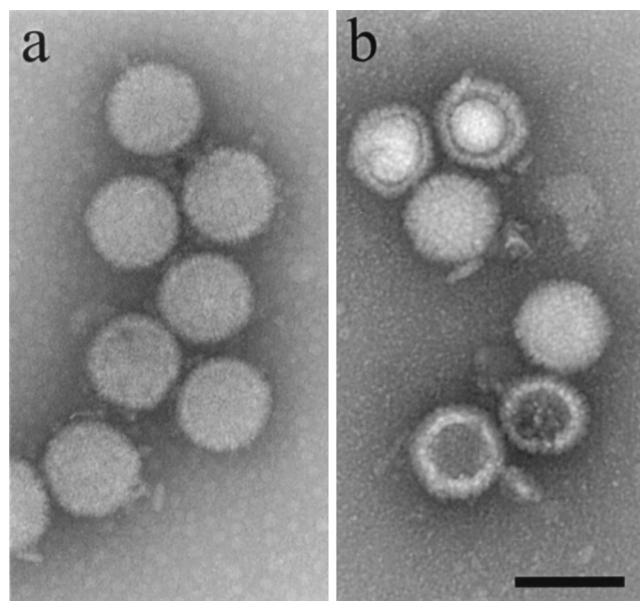


FIG. 6. *tsProt.A* procapsids before (a) and after (b) incubation at 21°C for 72 h. Procapsids were isolated by antibody precipitation as described in Materials and Methods from BHK cells infected for 15 h at 39°C (the NPT). Note that before incubation (a) procapsids are round in profile, indicating they have not angularized, while after incubation (b) capsid profiles show angles indicating they have the mature, icosahedral structure. Bar = 1,500 Å.

responding to cellular actin (starred band in Fig. 7a), a protein not seen in procapsids precipitated from Sf9 cell extracts (24). Two further observations relate to interpretation of the presence of actin. First, analysis of 6F10 immune precipitates from uninfected BHK cells showed the same actin band (data not shown). Second, no evidence of procapsid-associated actin was observed in electron micrographs of procapsids or in the three-dimensional reconstructions (Fig. 2a and b). We suggest therefore that actin in procapsid precipitates may result from a cross-reaction of MAb 6F10 with BHK cell actin or with a protein bound to actin. As indicated above, the cross-reacting form of actin is expected to be present in BHK but not Sf9 cells.

**Scaffold structure: tentative localization of the protease and nature of procapsid building blocks.** The three-dimensional reconstructions of *m100* and *tsProt.A* procapsids showed no strongly contrasted features in the core region (data not shown). The same result was obtained earlier with procap-

TABLE 1. Effect of incubation at 0°C on the integrity of *m100* procapsids and wild-type HSV-1 B-capsids<sup>a</sup>

Incubation for 30 min at (°C):	Mean no./electron microscope field ± SD (n)	
	<i>m100</i> procapsids	HSV-1 B capsids
21	120 ± 18 (3)	178 ± 30 (n = 3)
0	4 ± 3 (4)	199 ± 45 (n = 4)

<sup>a</sup> The procedures described in Materials and Methods were used to isolate procapsids from BHK cells infected for 18 h with HSV-1 *m100* virus. The procapsid-containing precipitate was resuspended in 100 μl of PBS and divided into two aliquots, which were incubated at room temperature (21°C) or 0°C. Samples were then applied to electron microscope grids, negatively stained with 1% uranyl acetate, and photographed in the electron microscope. Procapsids were counted on electron microscope negatives which were recorded at a magnification of ×8,300. The same analysis was performed with wild-type HSV-1 B capsids which were prepared from infected BHK cells as previously described (27).

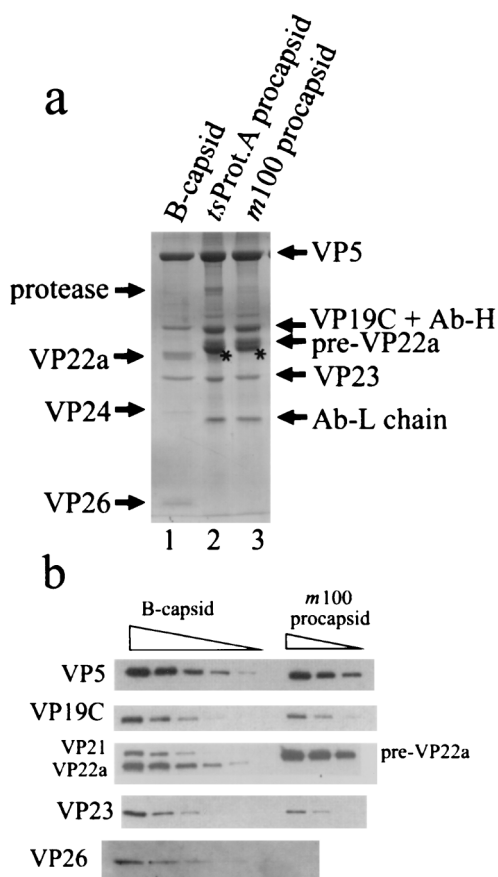


FIG. 7. Protein composition of HSV-1 procapsids. SDS-polyacrylamide gel electrophoresis of *m100* and *tsProt.A* procapsids was followed by staining with Coomassie blue (a) and Western immunoblotting with specific antibodies (b). Similar analyses of HSV-1 B-capsids are shown for comparison. The starred bands in lanes 2 and 3 of panel a were identified as actin as described in the text. The positions of the HSV-1 protease (UL26 gene product) and the antibody heavy and light chains (Ab-H and Ab-L) are indicated in panel a. Specimens in panel b were loaded for electrophoresis in twofold dilutions. The amount of sample loaded in the VP26 row was twofold greater than that loaded in other rows. Note that procapsid bands identified as VP5, VP19C, pre-VP22a, and VP23 were stained with specific antibodies, and VP26 was not detected in either *m100* or *tsProt.A* procapsids.

sids assembled in vitro (24, 46). As we would expect such features to be visible at the resolution now reached (18 Å), we conclude it is unlikely that the scaffold has highly ordered, icosahedrally symmetric features as the shell does. The absence of icosahedral ordering in the core is consistent with the suggestion made earlier (46) that the scaffold is organized as a protein micelle in which individual scaffold molecules are highly extended and arranged radially with their C termini attached to the shell and N termini extending inward toward the procapsid center.

More revealing information about the structure of the core was obtained from the radial density profiles shown in Fig. 5. In the region corresponding to the scaffolding protein (i.e., between radial distances of 180 and 480 Å), procapsids assembled in vitro showed three peaks of density interpreted earlier to correspond to three condensed scaffolding protein domains separated by flexible linkers (46). The same three peaks of density are readily identifiable in the profiles of *m100* and *tsProt.A* procapsids (Fig. 4), suggesting that the basic arrangement of the scaffold is the same in the three procapsid types.

In the innermost region of the core, at a radial distance of

less than 180 Å, the density profile computed for *tsProt.A* procapsids shows a large peak of density that is absent in *m100* and in vitro procapsids (Fig. 5). This peak suggests itself as the location of the maturational protease (UL26 gene product), as the protease is found in *tsProt.A* but not in *m100* or in vitro procapsids (Fig. 7a). Further studies, perhaps with mutants containing deletions in the UL26 gene, should be carried out to confirm this presumptive location for the protease.

The scaffolding protein content of *m100* procapsids was determined quantitatively from stained SDS-polyacrylamide gels and from integration of the scaffolding protein region in the three-dimensional reconstruction. The values obtained,  $1,918 \pm 170$  and  $1,866$  to  $2,070$  copies per procapsid respectively, are in good agreement with each other and with the scaffolding protein content of procapsids assembled in vitro (Table 2). Compared to other virus procapsids, the amount of *m100* procapsid scaffolding protein appears high. For example, the molar ratio of scaffolding to major capsid protein in *m100* procapsids is approximately 2.0 (i.e.,  $1,918 \pm 170$  scaffold:960 VP5 molecules), while the comparable values for the procapsids of phages P22,  $\phi 29$ , and T4 are 0.71 (300 scaffold:420 capsid), 0.9 (180 scaffold:200 capsid), and 0.67 (640 gp22 plus gp21:960 major capsid), respectively (2, 18, 31). The greater number of scaffolding protein molecules in HSV-1 procapsids may be necessitated by the larger major capsid protein (VP5 molecular weight of  $\sim 150,000$ , compared with 47,500, for instance, for the phage P22 coat protein, gp5) or perhaps by the greater diameter of the HSV-1 procapsid ( $\sim 126$  nm, compared with 58 nm for the P22 phage procapsid [29]). For example, despite the greater diameter of the HSV-1 procapsid compared to that of phage P22, the amounts of scaffolding protein per unit of volume are similar in the two, calculated values being 0.21 and 0.15 kDa/nm<sup>3</sup> for HSV-1 and P22, respectively (assuming that HSV-1 and P22 procapsid cavities have diameters of 950 and 450 Å).

The molar ratio of approximately 1 VP5:2 scaffolding molecules observed in the *m100* procapsid may provide a clue about the nature of the subunit(s) used in procapsid growth. Since the procapsid could be formed from subunits with the same molecular proportions as the completed structure, assembly units with a 1:2 VP5:scaffolding protein molar ratio are suggested. It is relevant to note therefore that sucrose gradient studies of the VP5-scaffolding protein interaction revealed complexes containing 1 VP5 plus 2 scaffold molecules and 2 VP5 plus 4 scaffold molecules (25). Both complexes are attractive as potential procapsid assembly units.

TABLE 2. Procapsid scaffolding protein content measured from three-dimensional reconstructions

Procapsid source	Scaffold mass (MDa) <sup>a</sup>	Scaffold protein copy no. <sup>b</sup>	Reference
Assembled in vitro in cell extracts	66.4–76.7	1,967–2,272	46
Assembled in vitro from purified proteins	75.8	1,902	25
Isolated from <i>m100</i> -infected cells	63.0–69.9	1,866–2,070	This study

<sup>a</sup> Determined by integration of radial electron density profiles such as those shown in Fig. 4. Ranges of values are shown for reconstructions in which there was uncertainty regarding the baseline in the radial density profile. The scaffold mass was calibrated relative to the shell mass, which was assumed to be 180.9 MDa (i.e., 960, 320, and 640 copies of VP5, VP19C, and VP23, respectively).

<sup>b</sup> Calculated by assuming the following molecular weights: for preVP22a, 33,760 (cell extract) and *m100* procapsids); for pUL80.5-H, 39,855 (purified protein procapsids).

The pre-VP22a content of *m100* procapsids (i.e.,  $1,918 \pm 170$  copies per procapsid) was found to be significantly higher than the content determined earlier of VP22a in HSV-1 B-capsids ( $1,153 \pm 169$  copies per capsid [27]). This observation suggests some of the scaffolding protein is lost from the procapsid as it matures to form the B capsid.

**Procapsid maturation.** Isolation of procapsids from *m100*- and *tsProt.A*-infected cells as described here suggests that procapsids may function *in vivo* in the same way they do *in vitro*, as precursors to the mature capsid form. As an overall measure of the ability of *m100* and *tsProt.A* procapsids to undergo further development, they were tested *in vitro* for the ability to be transformed into the icosahedral capsid morphology. Tests showed that both procapsid types were able to mature (Fig. 6), with a high proportion being transformed in each case. We interpret the results to support the view that procapsids function as assembly intermediates *in vivo*. The time required for transformation at 21°C, however, was longer than is expected in infected cells. For example, 60 to 72 h were required for procapsid transformation *in vitro* whereas in extracts maturation was complete in 8 h (24), and in infected cells the same process requires less than 3 h (5). We conclude that while *m100* and *tsProt.A* procapsids are capable of maturation *in vitro*, the rate of transformation *in vivo* is enhanced by some factor(s) not present in our *in vitro* incubations. Absence of the protease may account for at least part of the delay in the case of *m100* procapsids. With *tsProt.A* procapsids, the time required for thermoreversion of the protease may contribute to the observed delay. Packaging of virus DNA *in vivo* may also be involved in promoting the transformation from the procapsid to the mature capsid structure.

It is now clear that the overall pathway of HSV-1 capsid formation has important similarities to that observed in dsDNA bacteriophage such as P22, T4,  $\phi 29$ , and  $\lambda$  (4, 13, 31). For instance in dsDNA phage, capsid formation involves a scaffolding protein, and it proceeds by way of a spherical, more fragile procapsid intermediate. DNA is packaged into an empty phage capsid, and in most cases where the process has been well studied, packaging is found to be initiated with the procapsid whose shell matures into the icosahedral form before packaging is completed (14, 16, 17, 19, 37; but see reference 32). If HSV-1 DNA packaging also conforms to the phage model, then in the future it may be productive to examine the role of HSV-1 procapsids in initiation of DNA encapsidation.

#### ACKNOWLEDGMENTS

We thank David Burkwall, Oneida Mason, Min Gao, David Belnap, Geoffrey Williams, and James Conway for help and advice during the course of this study. We are also most grateful to Gary Cohen and Richard Courtney for providing antibodies specific for HSV-1 capsid proteins.

This work was supported in part by NIH grants AI41644 and AI37549 and by NSF grant MCB 9904879.

#### REFERENCES

- Baker, T. S., and R. H. Cheng. 1996. A model-based approach for determining orientations of biological molecules imaged by cryoelectron microscopy. *J. Struct. Biol.* **116**:120–130.
- Black, L. W., M. K. Showe, and A. C. Steven. 1994. Morphogenesis of the T4 head, p. 218–258. *In* J. D. Karam (ed.), *Bacteriophage T4*. ASM Press, Washington, D.C.
- Booy, F. P., B. L. Trus, W. W. Newcomb, J. C. Brown, J. F. Conway, and A. C. Steven. 1994. Finding a needle in a haystack: detection of a small protein (the 12-kDa VP26) in a large complex (the 200-MDa capsid of herpes simplex virus). *Proc. Natl. Acad. Sci. USA* **91**:5652–5656.
- Casjens, S., and R. Hendrix. 1988. Control mechanisms in dsDNA bacteriophage assembly, p. 15–91. *In* R. Calendar (ed.), *The bacteriophages*. Plenum Press, New York, N.Y.
- Church, G. A., and D. W. Wilson. 1997. Study of herpes simplex virus maturation during a synchronous wave of assembly. *J. Virol.* **71**:3603–3612.
- Conway, J. F., B. L. Trus, F. P. Booy, W. W. Newcomb, J. C. Brown, and A. C. Steven. 1996. Visualization of three-dimensional density maps reconstructed from cryo-electron micrographs of viral capsids. *J. Struct. Biol.* **116**:200–208.
- Dasgupta, A., and D. W. Wilson. 1999. ATP depletion blocks herpes simplex virus DNA packaging and capsid maturation. *J. Virol.* **73**:2006–2015.
- Desai, P., N. A. DeLuca, and S. Person. 1998. Herpes simplex virus type 1 VP26 is not essential for replication in cell culture but influences production of infectious virus in the nervous system of infected mice. *Virology* **247**:115–124.
- Engvall, E., and P. Perlman. 1971. Enzyme-linked immunosorbent assay (ELISA): quantitative assay for immunoglobulin. *Immunochemistry* **8**:871–874.
- Ey, P. L., S. J. Prowse, and C. R. Jenkin. 1978. Isolation of pure IgG1, IgG2a and IgG2b immunoglobulins from mouse serum using protein A-sepharose. *Immunochemistry* **15**:429–436.
- Fuller, S. D., S. J. Butcher, R. H. Cheng, and T. S. Baker. 1996. Three-dimensional reconstruction of icosahedral particles—the uncommon line. *J. Struct. Biol.* **116**:48–55.
- Gao, M., L. Matusick-Kumar, W. Hurlburt, S. F. DiTusa, W. W. Newcomb, J. C. Brown, P. J. McCann III, I. Deckman, and R. J. Colonna. 1994. The protease of herpes simplex virus type 1 is essential for functional capsid formation and viral growth. *J. Virol.* **68**:3702–3712.
- Hendrix, R. W. 1985. Shape determination in virus assembly: the bacteriophage example, p. 169–203. *In* S. Casjens (ed.), *Virus structure and assembly*. Jones and Bartlett Publishers, Inc., Boston, Mass.
- Hohn, B., and T. Hohn. 1974. Activity of empty, headlike particles for packaging of DNA in bacteriophage lambda *in vitro*. *Proc. Natl. Acad. Sci. USA* **71**:2372–2376.
- Homa, F. L., and J. C. Brown. 1997. Capsid assembly and DNA packaging in herpes simplex virus. *Rev. Med. Virol.* **7**:107–122.
- Jardine, P. J., and D. H. Coombs. 1998. Capsid expansion follows the initiation of DNA packaging in bacteriophage T4. *J. Mol. Biol.* **284**:661–672.
- Jardine, P. J., M. C. McCormick, C. Lutze-Wallace, and D. H. Coombs. 1998. The bacteriophage T4 DNA packaging apparatus targets the unexpanded prohead. *J. Mol. Biol.* **284**:647–659.
- Lee, C. S., and P. Guo. 1995. *In vitro* assembly of infectious virions of double-stranded DNA phage  $\phi 29$  from cloned gene products and synthetic nucleic acids. *J. Virol.* **69**:5018–5023.
- Masker, W. E., and P. Serwer. 1982. DNA packaging *in vitro* by an isolated bacteriophage T7 procapsid. *J. Virol.* **43**:1138–1142.
- Matusick-Kumar, L., W. Hurlburt, S. P. Weinheimer, W. W. Newcomb, J. C. Brown, and M. Gao. 1994. Phenotype of the herpes simplex virus type-1 protease substrate ICP35 mutant virus. *J. Virol.* **68**:5384–5394.
- McNab, A. R., P. Desai, S. Person, L. L. Roof, D. R. Thomsen, W. W. Newcomb, J. C. Brown, and F. L. Homa. 1998. The product of the herpes simplex virus type 1 UL25 gene is required for encapsidation but not for cleavage of replicated viral DNA. *J. Virol.* **72**:1060–1070.
- McNabb, D. S., and R. J. Courtney. 1992. Identification and characterization of the herpes simplex virus type 1 virion protein encoded by the UL35 open reading frame. *J. Virol.* **66**:2653–2663.
- Newcomb, W. W., and J. C. Brown. 1989. Use of Ar<sup>+</sup> plasma etching to localize structural proteins in the capsid of herpes simplex virus type 1. *J. Virol.* **63**:4697–4702.
- Newcomb, W. W., F. L. Homa, D. R. Thomsen, F. P. Booy, B. L. Trus, A. C. Steven, J. V. Spencer, and J. C. Brown. 1996. Assembly of the herpes simplex virus capsid: characterization of intermediates observed during cell-free capsid assembly. *J. Mol. Biol.* **263**:432–446.
- Newcomb, W. W., F. L. Homa, D. R. Thomsen, B. L. Trus, N. Cheng, A. C. Steven, F. P. Booy, and J. C. Brown. 1999. Assembly of the herpes simplex virus procapsid from purified components and identification of small complexes containing the major capsid and scaffolding proteins. *J. Virol.* **73**:4239–4250.
- Newcomb, W. W., F. L. Homa, D. R. Thomsen, Z. Ye, and J. C. Brown. 1994. Cell-free assembly of the herpes simplex virus capsid. *J. Virol.* **68**:6059–6063.
- Newcomb, W. W., B. L. Trus, F. P. Booy, A. C. Steven, J. S. Wall, and J. C. Brown. 1993. Structure of the herpes simplex virus capsid: molecular composition of the pentons and the triplexes. *J. Mol. Biol.* **232**:499–511.
- Potete, A. R., V. Jarvik, and D. Botstein. 1979. Encapsulation of phage P22 DNA *in vitro*. *Virology* **95**:550–564.
- Prasad, B. V. V., P. E. Prevelige, E. Marietta, R. O. Chen, D. Thomas, J. King, and W. Chiu. 1993. Three-dimensional reconstruction of capsids associated with genome packaging in a bacterial virus. *J. Mol. Biol.* **231**:65–74.
- Preston, V. G., J. A. V. Coates, and F. J. Rixon. 1983. Identification and characterization of a herpes simplex virus gene product required for encapsidation of virus DNA. *J. Virol.* **45**:1056–1064.
- Prevelige, P. E., and J. King. 1993. Assembly of bacteriophage P22: a model for ds-DNA virus assembly. *Prog. Med. Virol.* **40**:206–221.
- Rao, V. B., and L. W. Black. 1985. DNA packaging of bacteriophage T4 proheads *in vitro*; evidence that prohead expansion is not coupled to DNA packaging. *J. Mol. Biol.* **185**:565–578.

33. **Rixon, F. J.** 1993. Structure and assembly of herpesviruses. *Semin. Virol.* **4**:135–144.
34. **Rixon, F. J., and D. McNab.** 1999. Packaging-competent capsids of a herpes simplex virus temperature-sensitive mutant have properties similar to those of in vitro-assembled procapsids. *J. Virol.* **73**:5714–5721.
35. **Roizman, B., and A. E. Sears.** 1996. Herpes simplex viruses and their replication, p. 2231–2295. *In* B. N. Fields, D. M. Knipe, P. M. Howley, R. M. Chanock, J. L. Melnick, T. P. Monath, B. Roizman, and S. E. Straus (ed.), *Fields virology*. Lippincott-Raven, Philadelphia, Pa.
36. **Salmon, B., and J. D. Baines.** 1998. Herpes simplex virus DNA cleavage and packaging: association of multiple forms of UL15-encoded proteins with B capsids requires at least the UL6, UL17, and UL28 genes. *J. Virol.* **72**:3045–3050.
37. **Shibata, H., H. Fujisawa, and T. Minagawa.** 1987. Characterization of the bacteriophage T3 DNA packaging reaction in vitro in a defined system. *J. Mol. Biol.* **196**:845–851.
38. **Sodeik, B., M. W. Ebersold, and A. Helenius.** 1997. Microtubule-mediated transport of incoming herpes simplex virus 1 capsids to the nucleus. *J. Cell Biol.* **136**:1007–1021.
39. **Spencer, J. V., B. L. Trus, F. P. Booy, A. C. Steven, W. W. Newcomb, and J. C. Brown.** 1997. Structure of the herpes simplex virus capsid: peptide A862-H880 of the major capsid protein is displayed on the rim of the capsomer protrusions. *Virology* **228**:229–235.
40. **Steven, A. C., C. R. Roberts, J. Hay, M. E. Bisher, T. Pun, and B. L. Trus.** 1986. Hexavalent capsomers of herpes simplex virus type 2: symmetry, shape, dimensions, and oligomeric status. *J. Virol.* **57**:578–584.
41. **Steven, A. C., and P. G. Spear.** 1996. Herpesvirus capsid assembly and envelopment, p. 312–351. *In* R. Burnett, W. Chiu, and R. Garcea (ed.), *Structural biology of viruses*. Oxford University Press, New York, N.Y.
42. **Tatman, J. D., V. G. Preston, P. Nicholson, R. M. Elliott, and F. J. Rixon.** 1994. Assembly of herpes simplex virus type 1 capsids using a panel of recombinant baculoviruses. *J. Gen. Virol.* **75**:1101–1113.
43. **Taus, N. S., and J. D. Baines.** 1998. Herpes simplex virus 1 DNA cleavage/packaging: the UL28 gene encodes a minor component of B capsids. *Virology* **252**:443–449.
44. **Thomas, D., W. W. Newcomb, J. C. Brown, J. S. Wall, J. F. Hainfeld, B. L. Trus, and A. C. Steven.** 1985. Mass and molecular composition of vesicular stomatitis virus: a scanning transmission electron microscopy analysis. *J. Virol.* **54**:598–607.
45. **Thomsen, D. R., L. L. Roof, and F. L. Homa.** 1994. Assembly of herpes simplex virus (HSV) intermediate capsids in insect cells infected with recombinant baculoviruses expressing HSV capsid proteins. *J. Virol.* **68**:2442–2457.
46. **Trus, B. L., F. L. Homa, F. P. Booy, W. W. Newcomb, D. R. Thomsen, N. Cheng, J. C. Brown, and A. C. Steven.** 1995. Herpes simplex virus capsids assembled in insect cells infected with recombinant baculoviruses: structural authenticity and localization of VP26. *J. Virol.* **69**:7362–7366.
47. **Trus, B. L., F. P. Booy, W. W. Newcomb, J. C. Brown, F. L. Homa, D. R. Thomsen, and A. C. Steven.** 1996. The herpes simplex virus procapsid: structure, conformational changes upon maturation, and roles of the triplex proteins VP19C and VP23 in assembly. *J. Mol. Biol.* **263**:447–462.
48. **Trus, B. L., R. B. Roden, H. L. Greenstone, M. Vrhel, J. T. Schiller, and F. P. Booy.** 1997. Novel structural features of bovine papillomavirus capsid revealed by a three-dimensional reconstruction to 9 Å resolution. *Nat. Struct. Biol.* **4**:413–420.
49. **Vernon, S., M. Ponce de Leon, G. Cohen, R. Eisenberg, and B. Rubin.** 1981. Morphological components of herpesvirus. III. Localization of herpes simplex virus type 1 nucleocapsid polypeptides by immune electron microscopy. *J. Gen. Virol.* **54**:39–46.
50. **Whitley, R. J.** 1996. Herpes simplex viruses, p. 2297–2342. *In* B. N. Fields, D. M. Knipe, P. M. Howley, R. M. Chanock, J. L. Melnick, T. P. Monath, S. E. Straus, and B. Roizman (ed.), *Fields' virology*. Lippincott-Raven, Philadelphia, Pa.
51. **Yu, D., and S. K. Weller.** 1998. Herpes simplex virus type 1 cleavage and packaging proteins UL15 and UL28 are associated with B but not C capsids during packaging. *J. Virol.* **72**:7428–7439.
52. **Zhou, Z. H., B. V. V. Prasad, J. Jakana, F. J. Rixon, and W. Chiu.** 1994. Protein subunit structures in the herpes simplex virus capsid determined from 400-kV spot-scan electron cryomicroscopy. *J. Mol. Biol.* **242**:456–469.
53. **Zhou, Z. H., J. He, J. Jakana, J. D. Tatman, F. J. Rixon, and W. Chiu.** 1995. Assembly of VP26 in herpes simplex virus-1 inferred from structures of wild-type and recombinant capsids. *Nat. Struct. Biol.* **2**:1026–1030.
54. **Zlotnick, A., N. Cheng, J. F. Conway, F. P. Booy, A. C. Steven, S. J. Stahl, and P. T. Wingfield.** 1996. Dimorphism of hepatitis B virus capsids is strongly influenced by the C-terminus of the capsid protein. *Biochemistry* **35**:7412–7421.